Check for updates

Original Article

Hydranencephaly and porencephaly predominated among neuropathologic findings in stillborn and neonatal piglets during the first major outbreak of Japanese encephalitis in Australia

Veterinary Pathology
1–14
© The Author(s) 2026
Article reuse guidelines:
sagepub.com/journals-permissions
DOI: 10.1177/03009858261423130
journals.sagepub.com/home/vet
Sage

Willy W. Suen[1], Anne Jordan[2], Leah K. Manning[2], Selina Ossedryver[3], Shirley A. Turner[3], Graeme Knowles[4], Effie Lee[3,4], Zoe Spiers[2], Angel L. Ngo[2], Mark Hazelton[2], Deborah Finlaison[2], Peter Kirkland[2], Cathy Shilton[5], Jean Payne[1], Jennifer Harper[1], Kate Maynard[1], Yangchen Gurung[1], Teresa Eastwood[1], Tristan Reid[1], David T. Williams[1], Richard Ploeg[1], John Bingham[1,5], Brian A. Summers[6], and Pedro Pinczowski[2]

Abstract

In 2022, piggeries in southeastern Australia experienced an increase in reproductive losses and occasional neurologic disease in neonates with up to 100% mortality in some litters. Molecular testing identified a genotype IV Japanese encephalitis virus (JEV) as the etiological agent, detected for the first time in Australia. Necropsy of 235 JEV-positive domestic piglets, mostly stillbirths with 30% mummified, revealed hydranencephaly-porencephaly impacting the dorsal cerebrum as the most common lesion. Microscopically, this was characterized by varying degrees of parenchymal collapse as a result of liquefactive necrosis, hypoplasia, and dysplasia, with nonsuppurative inflammation and mineralization. In the most severe cases, hydranencephaly reduced the cerebral parenchyma to a thin membrane enclosing dilated lateral ventricles. Histologically, the affected neuroparenchyma was largely devoid of mature neurons, axons, myelin, and oligodendrocytes. What remained was mostly a dense population of IBA-1-positive histiocytes and few CD3-positive T-lymphocytes, interspersed within a dense network of GFAP-positive astrocytic processes. Immunohistochemistry for flaviviral antigen showed colocalization of viral antigen-positive neurons and necrotic foci. In less severe cases, cerebral necrosis occurred in well-demarcated, locally extensive regions or isolated gyri, sometimes with a vascular distribution, resulting in porencephaly. In addition, vascular calcification was noted, although with unknown significance and pathogenesis. Arthrogryposis, scoliosis, and kyphosis were observed in a small subset of the cases, which had myelodysplasia. Myelodysplastic changes varied and included central canal duplication, dysplastic gray matter, and bifurcation of the ventral medial sulcus. Multifocal necrosis and inflammation were also observed in the spinal cord, although the extent was typically limited.

Keywords

encephalitis, hydranencephaly, Japanese encephalitis virus, neuropathology, piglets, porencephaly, stillbirth

[1]CSIRO, Australian Centre for Disease Preparedness, Geelong, VIC, Australia
[2]Department of Primary Industries and Regional Development, Elizabeth Macarthur Agricultural Institute, Menangle, NSW, Australia
[3]Department of Primary Industries, Biosecurity Sciences Laboratory, Brisbane, QLD, Australia
[4]VETLAB Gribbles Veterinary Pathology, Glenside, SA, Australia
[5]Department of Agriculture and Fisheries, Berrimah Veterinary Laboratory, Berrimah, NT, Australia
[6]Melbourne Veterinary School, Melbourne University, Melbourne, VIC, Australia

Supplemental material for this article is available online.

Corresponding Authors:
Willy W. Suen, CSIRO, Australian Centre for Disease Preparedness, Geelong, VIC 3220, Australia.
Email: Willy.Suen@csiro.au

Pedro Pinczowski, Department of Primary Industries and Regional Development, Elizabeth Macarthur Agricultural Institute, Woodbridge Road, Menangle, NSW 2568, Australia.
Email: pedro.pinczowski@dpi.nsw.gov.au

Japanese encephalitis virus (JEV) is a mosquito-borne orthoflavivirus (*Orthoflavivirus japonicum*) with 5 recognized genotypes. JEV can cause severe encephalitis in humans[23,47] and horses,[12] and significant reproductive disease in pigs.[11,45,50,54] The virus is prevalent in south and south-east Asia and the western Pacific,[5,24] including countries neighboring Australia (Indonesia, Philippines, and Papua New Guinea). JEV genotypes I and II had been detected sporadically in the Torres strait and Cape York Peninsula in far north-eastern Australia in humans, sentinel pig herds, and mosquitos,[15,16,37,52,53] likely originating from Papua New Guinea,[40] but the virus was not believed to have become established in natural transmission cycles on mainland Australia.[52]

From February to May 2022, JEV genotype IV was detected in clinically affected commercial pig populations across large areas of southeastern Australia, which was previously free of JEV.[26] These areas included the states of New South Wales, Queensland, Victoria, and South Australia. The same JEV strain was also detected in feral pig populations in the Northern Territory, Queensland, and South Australia.[19,25] Clinically, JEV genotype IV caused widespread reproductive losses in pregnant sows and severe neurological disease in neonatal piglets. There were also 46 human, 1 alpaca, and several suspected equine cases during this outbreak.[19,26,29]

Histopathological changes seen with naturally or experimentally infected juvenile and adult mice, pigs, dogs, nonhuman primates, and humans are well documented. Affecting most brain regions, these changes include nonsuppurative encephalitis and meningoencephalitis with perivascular cuffing, neuronal necrosis, neuronophagia, astrocytosis, gliosis, and glial nodules.[10,13,14,17,18,20,30,31,43,55] There is a paucity of literature describing the gross and histological changes seen in fetuses infected in utero.

Outbreaks of JEV in pigs have been described since the 1940s.[51] Nonsuppurative encephalitis in fetuses and stillborn piglets was attributed to JEV during an outbreak in Japan in 1948.[51] More recently in 2005 in India, gross changes in stillborn piglets infected with JEV genotype III included hydranencephaly, ventricular dilation with thinning of the parenchyma, as well as loss of gyri and sulci.[11] Hydranencephaly refers to a near-total loss or absence of the cerebral hemispheres in fetuses due to the destruction of formed neocortical elements and immature neural cells critical for normal neurodevelopment.[9,48] Porencephaly refers to a more focal to regional loss of the developing brain; [9,48] however, this has not been described in JEV-infected porcine fetuses. Histological changes reported in JEV-infected fetuses included neuronal degeneration, gliosis, perivascular cuffing, edema, congestion and hemorrhage, with immunohistochemistry (IHC) demonstrating the presence of JEV antigen mainly in cerebral neuronal cytoplasm.[11] This study aims to add to this existing but limited body of knowledge by conducting a comprehensive characterization of the gross and histopathologic changes in the central nervous system (CNS) seen in porcine fetuses naturally infected in utero with JEV-genotype IV during the 2022 Australian outbreak. Through this report, we aim to educate veterinary and one health professionals to recognize key features of this disease, aiding early detection of future outbreaks.

Materials and Methods

Case Materials

The case materials presented in this study were submitted from February to May 2022 to the Australian Centre for Disease Preparedness (ACDP), and to 4 Australian state/territory level veterinary laboratories, namely Elizabeth Macarthur Agricultural Institute (EMAI) from New South Wales; Biosecurity Sciences Laboratory (BSL) from Queensland, Gribbles VETLAB from South Australia, and Berrimah Veterinary Laboratory from Northern Territory. Included in this study were 235 domestic piglets submitted for necropsy (46 to ACDP, 108 to EMAI, 78 to BSL, and 3 to Gribbles VETLAB) that tested positive for JEV by a reverse transcriptase quantitative polymerase chain reaction (RT-qPCR). Most were stillbirths, while some presented with aerated lungs, consistent with neonatal piglets. In addition, we included one JEV RT-qPCR-positive feral porcine fetus from Berrimah Veterinary Laboratory retrieved from a JEV-positive feral sow that was terminated as part of a 2022 Northern Australian Quarantine Strategy surveillance program. The sow was apparently clinically normal, but positive for JEV by universal JEV TaqMan RT-qPCR testing of tonsil samples.

Necropsy

Routine postmortem examinations and specimen collection were performed on the piglets received at the 5 laboratories; protocols were similar but not identical (see below). At labs where testing was available, fresh tissue was collected and tested for JEV and other potential infectious causes. Samples included brain and a variety of other tissues. The brain and a variety of extraneural tissues from nonmummified piglets were collected and immersed in 10% neutral-buffered formalin for histologic processing. In addition, the entire vertebral column was collected and immersed in formalin in a subset of cases. Ethylenediaminetetraacetic acid decalcification was used to soften vertebral bone for further dissection to extract the spinal cord.

Histology

Extensive histologic investigation was undertaken on selected cases with macroscopic lesions by 2 laboratories in this study. ACDP pathologists examined at least 5 sections of the brain from 12 animals and 1 to 6 transverse and 1 to 2 parasagittal sections of the cervical, thoracic, and/or lumbar spinal cord from 11 animals across 6 batches of submissions; EMAI pathologists generally examined 1 to 3 sections of the brain from a total of 108 animals across 18 batches of submissions. Ad hoc histologic investigations were performed by the remaining laboratories.

Formalin-fixed tissues were processed, embedded in paraffin, sectioned, and stained with hematoxylin and eosin using standard methods.[2] Special histochemical stains, such as periodic acid-Schiff, Masson's trichrome, von Kossa, Luxol fast blue with Nissl counterstain (cresyl violet), and Bielschowski stains were performed as per methods described by Bancroft, Gamble.[3] Sections were digitized using Pannoramic Scan II (3DHISTECH Ltd; scanning resolution 0.27 μm/pixel) and Evident (Olympus) VS200 whole slide imager (scanning resolution 0.278 μm/pixel), and examined using Xplore (Phillips), CaseViewer (3DHISTECH Ltd), or OlyVIA 4.1.1 (Olympus) software. Photomicrographs were taken using the image capture function in Xplore, CaseViewer or OlyVIA.

Immunohistochemistry

Immunohistochemistry for viral antigen and cell marker detection was performed at ACDP. This was performed on all CNS sections from 24 animals. Each assay was optimized for maximum signal of the antigenic target and no to negligible background labeling in porcine CNS by the use of appropriate positive and negative controls. Once optimized, each batch of IHC of the test slides included a positive control (a flavivirus-infected brain for viral antigen IHC and, typically, normal fetal, postnatal and adult porcine brains, and/or lymph node for the cell marker IHCs) to ensure consistency in immunolabeling across batches.

Detection of flavivirus nonstructural 1 (NS1) protein in neural and extraneural tissue sections was achieved with a monoclonal antibody 4G4 (at 1:100) raised against the Murray Valley encephalitis virus NS1 protein (Prof. Roy Hall, University of Queensland). Extraneural tissues examined included kidney, liver, spleen, lung, trachea, thymus, lymph nodes, gastrointestinal tract, heart, gonads, and reproductive tracts. Detection of mature neurons, axons, oligodendrocytes, astrocytes, and histiocytes including microglial cells was achieved using antibodies against the mature neuronal marker NeuN (Abcam, Cat# ab177487, Dallas, Texas, at 1:100), phosphorylated axonal epitopes on neurofilament M and H proteins (clone SMI 312, Biolegend, San Diego, CA, Cat #837904, 1:1000), Olig2 (Abcam, Cambridge, MA, Cat# ab109186, at 1:100); glial fibrillary acidic protein (Dako Agilent Technologies, Singapore, Cat# Z0334, at 1:4500), and IBA-1 (Genetex, Cat# gtx100042, at 1:250), respectively. Anti-CD3 (Dako Agilent Technologies, Singapore, Cat# A0452, at 1:100) and anti-CD20 (Invitrogen Thermo Fisher Scientific, PA5-16701 Fremont, CA, at 1:400) antibodies were also used to identify T- and B-lymphocytes, respectively.

Prior to immunohistochemical labeling, antigen retrieval was performed using the Dako PT link and EnVision FLEX Target Retrieval Solution High pH (Agilent Technologies, Singapore, Cat #K8004) for 20 min at 97 °C. A 3% hydrogen peroxide (Chem-Supply, Cat # HA154-500M) solution in EnVision FLEX Peroxidase-Blocking reagent (Agilent Technologies, Singapore, Cat #K8002) was also used to eliminate endogenous peroxidase activity. The primary antibodies (as above) were applied for 1 hour at room temperature. A horseradish peroxidase-labeled secondary antibody, EnVision FLEX/ HRP (Agilent Technologies, Singapore, Cat #K8002), was then applied to all immunohistochemical sections followed by the chromogen AEC (PolyDetector Liquid AEC HRP, BioSB, Santa Barbara, CA, Cat# BSB0061; and Sigma AEC-tablets, St Louis, MO, Cat # SLBW3093), and was evident as a red-brown precipitate. For the 4G4 antibody, following application of the primary antibody, EnVision FLEX+ Mouse Linker (Agilent Technologies, Singapore, Cat #K8002) was routinely applied to amplify the signal. Under certain circumstances (eg, where 4G4 immunolabeling requires verification), a more stringent protocol without the use of EnVision FLEX+ Mouse Linker was used.

The density of cells positively labeled for viral NS1 antigen was evaluated and scored by one pathologist based on the strongest labeled focus within each of the neuroanatomic regions, using a 40× field of view (FOV) function in CaseViewer, which demarcated an area of approximately 0.304 mm^2 (Supplemental Fig. S1a–c). Areas with less than 10 positive cells per 40x FOV were assigned a score of 1, areas with 10–40 positive cells per 40× FOV were assigned a score of 2, and areas with more than 40 positive cells per 40× were assigned a score of 3. A score of zero represented a negative region.

Molecular Detection of JEV

Tissues were prepared as 10% (w/v) homogenates in Dulbecco's phosphate-buffered saline (pH 7.6; Oxoid) containing antibiotics (Sigma-Aldrich) using 1 mm silicon carbide beads (BioSpec Products) in a FastPrep24 tissue homogenizer (MP Biomedical, USA). Samples were clarified by low-speed centrifugation (1000 × *g*, 5 minutes, 4°C) and nucleic acid was extracted from supernatants using the MagMAX 96 Viral RNA Kit (ThermoFisher Scientific) in a MagMAX Express Magnetic Particle Processor (ThermoFisher Scientific), following the manufacturer's instructions. Reverse transcription quantitative polymerase chain reaction (RT-qPCR) testing was performed using a universal JEV-specific assay targeting the *NS1* gene of all 5 JEV genotypes.[44] Reactions contained 5 μl of RNA, 12.5 μl of AgPath One-step RT-PCR buffer (Ambion), 1 μl of 25X reverse transcriptase, 1.0 μl of 10 μM each primer (forward: 5′-GCCACCCAGGAGGTCCTT; reverse: 5′-CCCCAA AACCGCAGGAAT), 1.0 μl of 5 μM TaqMan probe (5′-FAM-CAAGAGGTGGACGGCC-MGB), and 3.5 μl of nuclease free water. Thermocycling conditions used were as follows: 10 minutes at 45°C for reverse transcription, 10 minutes at 95°C for inactivation of reverse transcriptase, followed by 45 cycles of 95°C for 15 seconds and 60°C for 45 seconds using a 7500 Real-time PCR system (Applied Biosystems) or QuantStudio 5 Real-time PCR system (ThermoFisher Scientific). Final cycle threshold (C_t) values are the mean of duplicate tests, with values less than 40 considered positive.

Statistical Analysis

All statistical analyses were performed using GraphPad Prism 5.0. A Spearman correlation analysis was performed on the

IHC scores assigned to the different CNS regions in 24 animals. These were compared against the C_t values of the corresponding fresh brain samples. A Kruskal-Wallis test with Dunn's multiple comparison posttest was performed on the C_t values of 211 fresh tissue samples to highlight sample types with significantly lower C_t values. Note, the C_t values from blood (n = 2), bladder (n = 1), stomach (n = 1), testicle (n = 1), and uterus (n = 1) were excluded from the statistical analysis due to a sample size of less than 3. Statistical significance was defined as a P value of less than .05 in both statistical tests.

Results

Clinical History

Commercial piggeries reported a clinical history of increased reproductive losses. Affected litters had varying degrees of fetal mortality, ranging from 30% to 100%. There were reports of significant variation in the size of piglets at birth in some litters. Mummification, stillbirths, and delayed farrowing were also commonly reported. Although rare, some piglets born alive exhibited neurologic signs, including paddling, tremors, and seizures.

Gross Pathologic Findings

The necropsy findings from a total of 235 JEV-positive domestic piglets from ACDP, EMAI, BSL, and Gribbles VETLAB were included in this study. The crown-to-rump length was measured in 105 animals, with a range of 8 to 38 cm, an average of 25.2 cm, and a median of 25.0 cm. Seventy piglets were mummified fetuses (30%). The brains of 184 piglets were examined for gross pathologic changes; 137 (74%) had varying degrees of hydranencephaly-porencephaly (Fig. 1a–d). The remaining 26% had no grossly observable lesions. In addition, 44 piglets had arthrogryposis (19%, Fig. 1e), 10 had kyphosis (4%, Fig. 1e), and 13 had scoliosis (6%, Fig. 1f). The one qRT-PCR positive fetus from a feral pig, which was killed at mid-gestation, had a crown-to-rump length of 12 cm, and did not exhibit any gross abnormalities.

The hydranencephaly observed in this outbreak was characterized by varying degrees of collapse of the cerebral hemispheres (Fig. 1a–d). In severe cases of hydranencephaly, which was common, the cerebral hemispheres were reduced to only a thin collapsed translucent membrane enclosing serosanguineous to clear fluid (Fig. 1a). The brain stem and cerebellum were mostly spared (Fig. 1a) but occasionally affected. In the milder cases, generally in animals with well-developed brains, patchy yellow discoloration consistent with malacia could be observed in the cerebral cortex (Fig. 1b). Porencephaly only became evident upon sectioning of the fixed brain (Fig. 1d). Tissue loss resulted in variable dilation of the lateral ventricles. In some hydranencephalic piglets, yellow mineralized material was found attached to the inner lining of the dilated lateral ventricles (Fig. 1c). The loss of nervous tissue and mineralization occasionally extended into the spinal cord (Fig. 1g–i), although dorsal root ganglia were consistently spared (Fig. 1h). Syringohydromyelia was present in one case.

Common extraneural lesions included generalized subcutaneous edema, clear serosanguineous cavitary effusions, serosal and mucosal petechiation, and peritesticular edema.

Histopathologic Findings

Brain lesions. Histologically, hydranencephaly was characterized by varying degrees of cerebrocortical parenchymal collapse accompanied by white matter rarefaction; coagulative or liquefactive necrosis; variable amount of hemorrhage with scattered accumulations of hematoidin and hemosiderin-laden macrophages; and inflammatory changes typical of viral infection, including a lymphohistiocytic meningeal and neuroparenchymal infiltrate, perivascular cuffs, neuronal satellitosis, and glial nodule formation (Fig. 2a–h and Supplemental Fig. S2a–c). Coagulative necrosis and mineralization of individual neurons were common (Fig. 2f), as were widespread liquefactive necrosis (Fig. 2c), rarefaction or vacuolation (Fig. 2a), and multifocal dystrophic mineralization within the neuroparenchyma (Fig. 2c, e; Supplemental Fig. S2b, f). While the dorsal cerebral cortex was most severely affected, regionally extensive necrosis in the thalamus was common (Fig. 2f). The olfactory cortex, cerebellum, and brainstem caudal to the midbrain were spared from significant necrosis in less severe cases. A focal cerebellar infarct was observed in one case (Supplemental Fig. S2e). The most common histologic changes observed in the brainstem were suggestive of atrophy, hypoplasia, and/or dysplasia (Supplemental Fig. S2f), noting that because this involved developing neural tissue, there were often significant overlaps between each of these disease processes, and differentiation of the individual processes by routine histology alone was difficult. Rarely, the JEV-positive fetal CNS presented without parenchymal collapse. Many of these grossly unremarkable cases had mild microscopic changes, such as multifocal neuronal necrosis and inflammatory changes.

Liquefactive necrosis of the neuroparenchyma was characterized by locally extensive to diffuse areas affected by loss of cellular detail with ultimate parenchymal lysis, cavitation, and replacement with foamy macrophages. The focal to regionally extensive cystic regions of necrosis in some animals were consistent with porencephaly (Fig. 2b, d; and Supplemental Fig. S2a, f). In some instances, the parenchymal loss incorporated subcortical and deeper white matter resulting in leukomalacia. Figure 2a and b, and Supplemental Fig. S2a illustrate mild, moderate, and severe cases of leukomalacia, respectively. The overlying gray matter may exhibit some degree of necrosis, atrophy, and/or hypoplasia. The necrotic areas in the hydranencephalic brains ranged from well-demarcated focal areas in a single gyrus to isolated cerebrocortical gyri (Fig. 2b) to the entire hemisphere (Fig. 2c, e). In some cases, the distribution of necrotic gyri corresponded to the distribution of particular cerebral blood vessels (eg, dorsomedial gyri of rostral cerebrum supplied by the rostral cerebral artery; Fig. 2b).

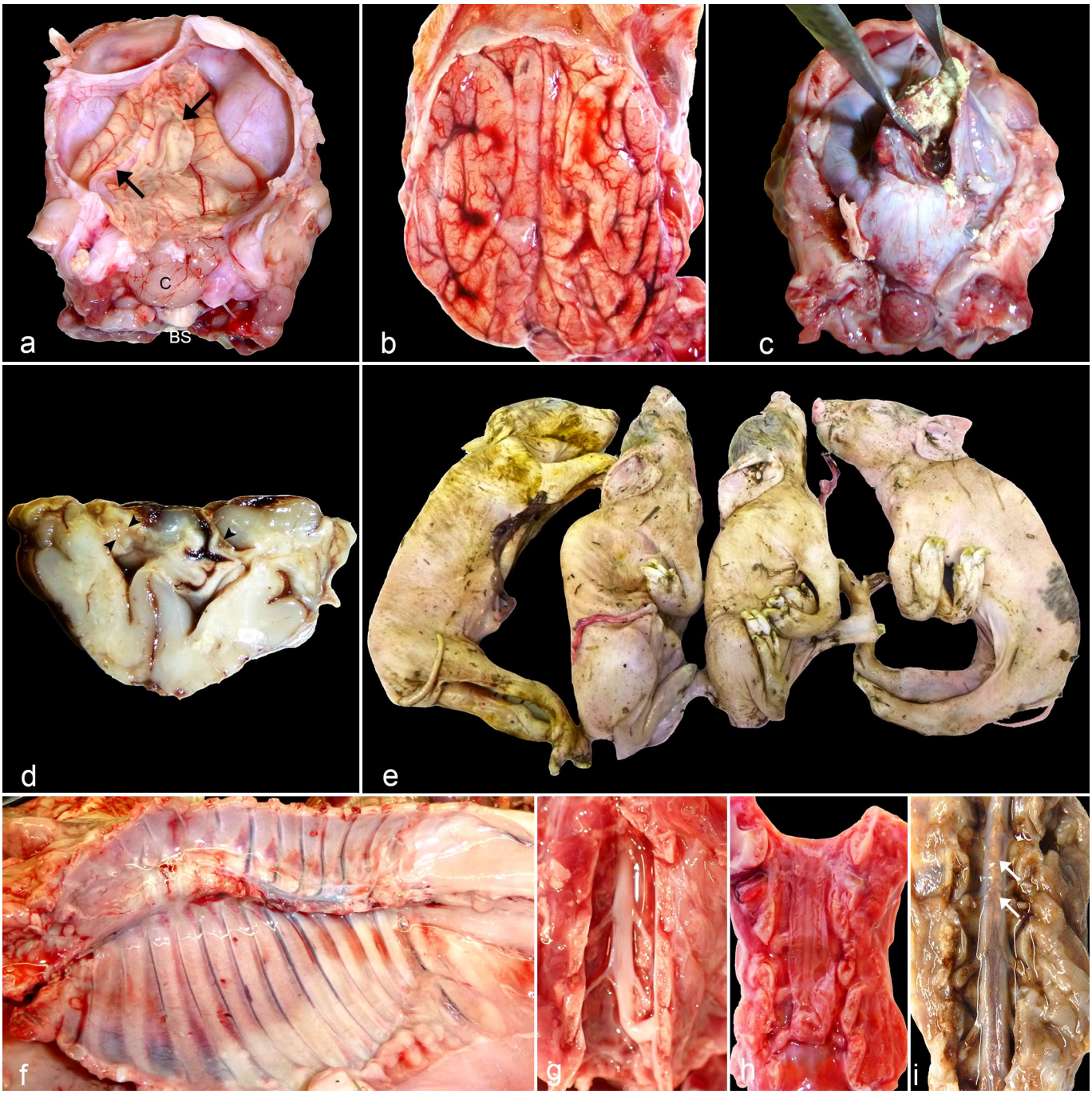

Figure 1. Most common gross findings in Japanese encephalitis virus (JEV)-positive piglets. (a) Brain. Much of the dorsal cerebrum has failed to develop, leaving only a thin pial-glial membrane (arrows indicate margins), which has collapsed and folded. The brainstem (BS) and cerebellum (C) are intact. This is the characteristic gross appearance of JEV-induced piglet hydranencephaly. (b) Brain. In marked contrast to (a), infrequently, brain development was not disrupted. In this brain, JEV infection is only evident as subtle changes, such as the yellow-tan discoloration in some gyri, particularly those in the right hemisphere, consistent with malacia. Microscopically, this was found to be due to necrosis. Brain swelling has produced mild flattening of the cerebral surface. (c) Brain with hydranencephaly. Incision into the opaque, gray dural membrane reveals only a thin remnant of the right caudal cerebrum with abundant light yellow granular material (mineralization) that is adhered to the inner aspect of the hydranencephalic cavity. (d) Transverse section of a fixed brain at the level of the septal nuclei. In contrast to the intact olfactory cortex, the dorsal neocortex has collapsed and 2 small porencephalic white matter cavities can be seen (arrowheads). (e) Stillborn piglets. JEV-infected piglets exhibit forelimb and hindlimb arthrogryposis and kyphosis of the thoracic spine. (f) Thoracic spine. There is marked scoliosis affecting the mid-portion of the thoracic spine. (g) Cervical spinal cord following laminectomy (dorsal view). The spinal cord is considerably reduced in size compared with the vertebral canal. This was interpreted as moderate hypoplasia/atrophy. (h) Cervical spinal cord following laminectomy (dorsal view). Only a very slender spinal cord is evident with retention of the pachymeninges and dorsal root ganglia. This was interpreted as marked hypoplasia/atrophy. (i) Formalin-fixed lumbar spinal cord following laminectomy (dorsal view). Coalescing tan foci (white arrows) are noted in the spinal cord, representing dystrophic mineral deposition.

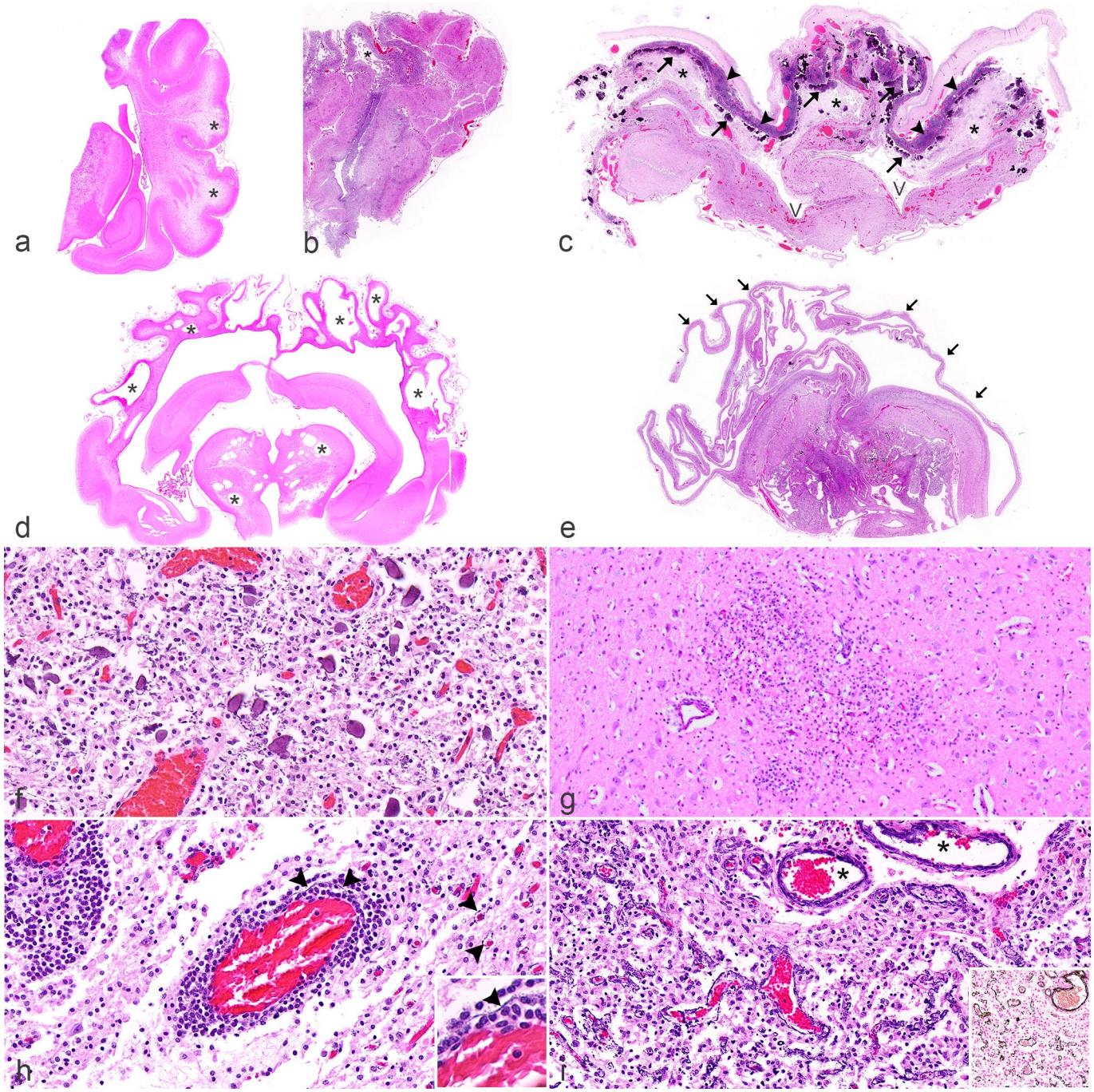

Figure 2. Brain and spinal cord histopathologic findings in Japanese encephalitis virus (JEV)-positive piglets. Hematoxylin and eosin. (a) Mid to caudal cerebrum, hippocampus, and thalamus. There is multifocal subcortical white matter rarefaction (*) occasionally associated with thinning of the overlying gray matter. A similar focal lesion with a minimal or mild inflammatory infiltrate is also noted in the thalamus. (b) Cerebrum, frontal lobe. The subcortical white matter in the dorsomedial gyrus is affected by necrosis and cavitation, interpreted as porencephaly (*). The increased basophilia of the residual gray matter is due to mononuclear cell hypercellularity and vascular mineralization. (c) Cerebrum, frontal lobe with emerging hydranencephaly. There is diffuse necrosis (*) with widespread multifocal mineralization of the dorsal cerebral cortex (arrows) and severe, mononuclear cell meningeal infiltrates (arrowheads). Furthermore, the absence of cerebral gyri and sulci is consistent with lissencephaly. "V" denotes lateral ventricles. (d) Mid to caudal cerebrum, hippocampus, and thalamus. Multiple porencephalic cysts (*) are evident in the cerebrum and diencephalon. The third and lateral ventricles are also dilated. (e) Mid to caudal cerebrum, hippocampus, and thalamus. The severely hydranencephalic cerebrum is reduced to a thin ribbon of tissue (arrows). In the diencephalon, there is severe necrosis, hemorrhage, and parenchymal mineralization. (f) Thalamus. Several mineralized neurons are admixed with a severe mononuclear leukocytic infiltrate. (g) Thalamus. There is locally extensive infiltrates of mononuclear leukocytes in the neuroparenchyma. (h) Thalamus. Mononuclear cells in perivascular cuffs trickle into the adjacent parenchyma. In the perivascular space of the vessel in the center and few capillaries in the right of the image, there is trace amount of linear basophilic mineral deposits (arrowheads). Inset: A higher magnification image of the linear mineral deposits (arrowhead) in the perivascular space of the vessel in the center. (i) Cerebral cortex and overlying meninges. Mural vascular mineralization in meningeal venules (*) and perivascular mineralization in intermediate- to small-caliber parenchymal vessels. Inset: von Kossa stain; argyrophilic material is consistent with mineral within and around the walls of blood vessels.

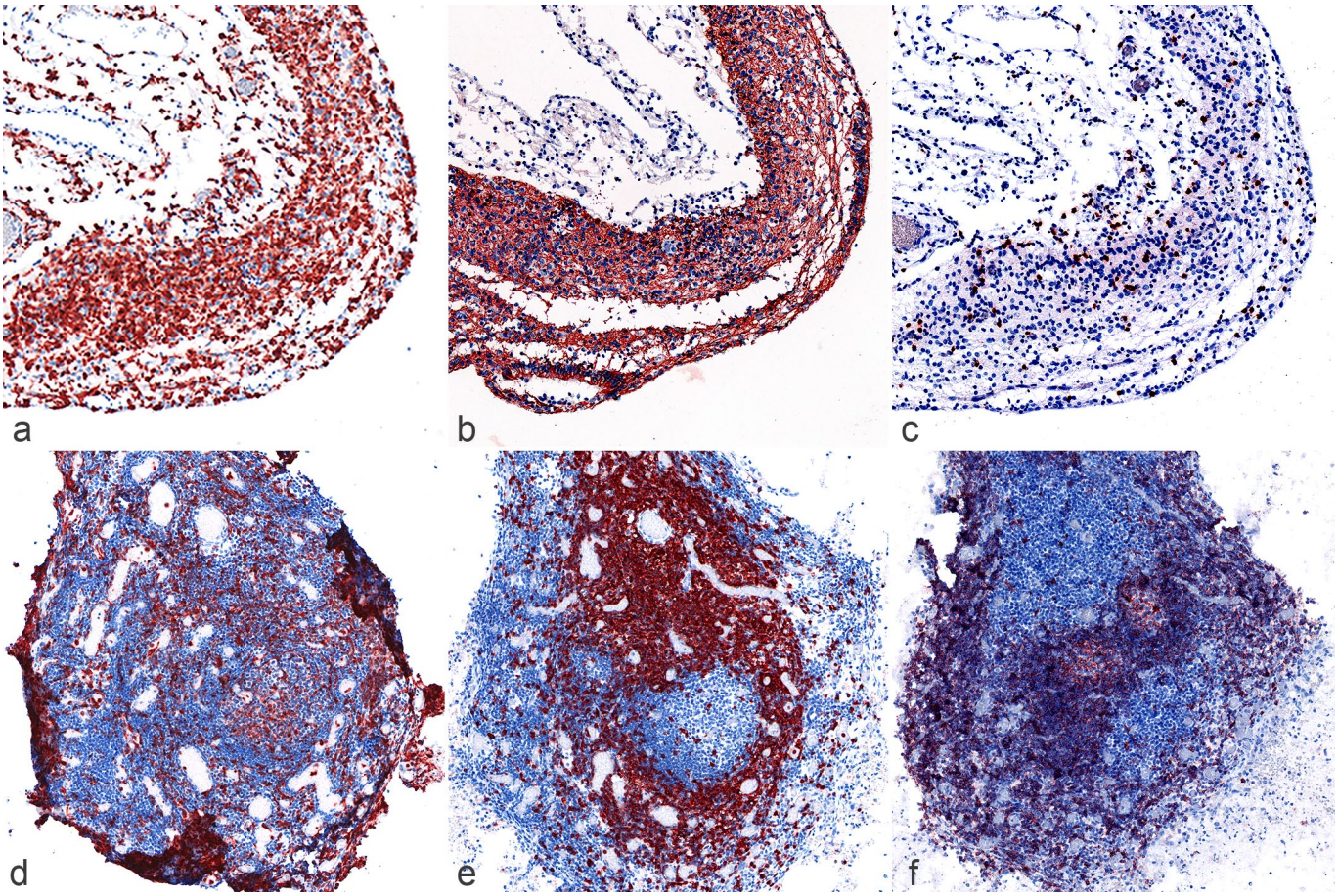

Figure 3. Immunophenotyping of cell types amidst the severely hydranencephalic cerebral cortex (a–c) and the meningeal infiltrate accompanying areas of cerebral cortical necrosis (d–f). Note the infiltrate represented in panels d–f was imaged from the base of a sulcus with the necrotic neuroparenchyma surrounding the 3 sides of the meningeal infiltrate. (a) Numerous microglial cells and/or infiltrating macrophages comprise the significantly depleted cerebral cortical parenchyma. IBA-1 immunohistochemistry (IHC). (b) A dense network of astrocytic processes is present in the affected parenchyma. Glial fibrillary acidic protein IHC. (c) Scattered CD3-positive T-lymphocytes are present in the affected parenchyma. CD3 IHC. (d) The mononuclear meningeal infiltrate is composed of a generalized infiltrate of monocytes-macrophages. IBA-1 IHC. (e) The mononuclear meningeal infiltrate also comprises numerous CD3-positive T-lymphocytes. Note the immunolabeled T-lymphocytes that surrounded and highlighted a focus of CD3-negative mononuclear cells, suggesting a lymphoid follicle. CD3 IHC. (f) CD20-positive B-lymphocytes form follicular structures in the center of the meningeal infiltrate, as well as diffusely distribute along the pial aspect of the meninges. CD20 IHC.

Multifocal ulceration of the ependyma was accompanied by ependymal rosettes and granulation, representing reactive or reparative changes. Such lesions were common throughout the ventricular system of the brain (Supplemental Fig. S2g, h).

In a subset of animals (8/12 of the ACDP cases; 8/108 of the EMAI cases), concurrent calcifying vasculopathy was observed in the brain and occasionally spinal cord (see the "Spinal cord lesions" section). The vasculopathy was characterized by basophilic granular and von Kossa-positive argyrophilic material consistent with mineral circumferentially deposited in or around blood vessels of the arterial and venous systems in the CNS (Fig. 2i and to a lesser extent 2h). Affected vessels ranged from large meningeal vessels (typically with intramural mineral deposits) to parenchymal capillaries (typically with perivascular deposits). Usually, the calcified parenchymal vessels were branches of mineralized meningeal vessels (Fig. 2i). There was no discernible predilection site for calcified vessels. While occasionally vascular calcification was observed in areas of parenchymal loss, this association was not always consistent. Notably, in most instances, mineralized vessels did not appear otherwise compromised, lacking either endothelial degeneration or thrombosis, even in areas with considerable vascular mineralization. Mural or perivascular mineralization was not observed in extraneural tissues, indicating this change was specific to the CNS.

Immunophenotyping of cell types in hydranencephalic cerebral parenchyma and mononuclear meningeal infiltrates. The extensive loss of parenchymal cell populations in the necrotic regions was clarified when IHC was performed (Fig. 3a–c; and Supplemental Fig. S3). Most notably, mature neurons, their myelinated axons, and most oligodendrocytes (Supplemental

Fig. S3b–f) were replaced by a dense mononuclear cell population, consisting of histiocytes (likely an admixture of predominantly infiltrating macrophages and to a lesser extent hypertrophied microglial cells; Fig. 3a), astrocytes and their fibrillary processes (Fig. 3b), and scattered CD3-positive T-lymphocytes (Fig. 3d). Scattered CD20-positive B-lymphocytes were only noted in the meninges (Supplemental Fig. S3a).

Widespread liquefactive necrosis of the neopallium was accompanied by a heavy mononuclear cell infiltrate in the overlying meninges. The infiltrate comprised many histiocytes (IBA-1-positive), admixed with T- and B-lymphocytes (CD3 and CD20-positive, respectively; Fig. 3d-f). The B-lymphocytes were organized into follicular structures (Fig. 3f).

Spinal cord lesions. In the spinal cord, histologic changes were generally limited to degeneration of individual neurons accompanied by satellitosis, neuronophagia (Fig. 4e), and glial nodules, although in some cases, the entire spinal cord was effaced by diffuse parenchymal necrosis, hemorrhage, mineralization, and inflammation (Fig. 4a). The vascular calcification observed in the brain was also occasionally noted in the spinal cord (Fig. 4f). There was often moderate reduction in the number of neurons, likely representing loss or aplasia, such as from viral-induced apoptosis or a disturbance in normal development.

At the subgross level, the diameter of the spinal cord was commonly decreased (n = 5 of 11), sometimes to the size of a dorsal root ganglion or smaller, consistent with hypoplasia and/or atrophy (Fig. 4b). This change was interpreted as micromyelia. Another relatively common lesion in the spinal cord was duplication of the central canal and bifurcation of the ventral median fissure (Fig. 4c). The spinal cord gray matter was often dysplastic with incomplete lateral separation of dorsal and/or ventral horns (Fig. 4c). Together, these changes were consistent with myelodysplasia (n = 5 of 11). All 5 animals with myelodysplasia had arthrogryposis; 3 had scoliosis and 3 had kyphosis. Animals without spinal cord malformation did not have any joint changes (n = 6 of 11), indicating a possible association between arthrogryposis and myelodysplasia, and to a lesser extent between the vertebral changes and the myelodysplasia. The one case with syringohydromyelia was characterized by a large cavitating lesion effacing much of the dorsal half of the spinal cord parenchyma (Fig. 4d). The cavity comprised multiple communicating compartments, some of which were partially lined by ependymal cells suggesting involvement of the central canal (Fig. 4d, inset).

Viral Antigen IHC

IHC targeting flaviviral NS1 was performed on brain and spinal cord sections from 24 JEV-positive domestic porcine fetuses and 1 feral porcine fetus. The latter was excluded from statistical analyses, as it was collected in mid-gestation before having reached a clinical end-point, in contrast to the domestic counterparts. Most fetuses had a low viral antigen score of one (less than 10 positive cells per 40× FOV in the focus with the strongest labeling, Figs. 5a and 6a). It was common for severely atrophied, hypoplastic, or dysplastic regions to be viral antigen negative. When present, antigen-positive cells were often in an advanced state of degeneration (Fig. 5a). Antigen labeling could also be detected in cellular debris found within mineralized foci, colocalizing viral infection and necrosis (Fig. 5b). Viral antigen was most frequently detected and densest in the dorsal cerebral cortex where hydranencephaly and porencephaly were most pronounced (Fig. 6a).

Antigen was detected in morphologically intact neurons in rare cases (Fig. 5d). These were generally seen in association with acute to subacute multifocal inflammatory changes, such as neuronal satellitosis, neuronophagia, glial nodules, and mononuclear parenchymal infiltrate. Antigen-positive neurons were also detected in the thalamus, midbrain, and lumbar spinal cord (Fig. 6a). Viral antigen was not detected in extraneural tissues, such as kidney, liver, spleen, lung, trachea, thymus, lymph node, gastrointestinal tract, heart, gonad, and reproductive tract, although some of these tissues tested positive by RT-qPCR.

Molecular Detection of JEV

An analysis of C_t values from JEV RT-qPCR testing was conducted using 211 postmortem samples to identify ones with the lowest C_t values corresponding to the highest viral RNA loads. The analysis showed that the brain and placenta were the 2 sample types with the lowest median C_t values (brain: 26.4 [range: 15–37]; placenta: 24.5 [range: 23–27]; Fig. 6b). These medians were significantly lower than the those of the heart, thoracic fluid, spleen, lung, kidney, and liver (Fig. 6b). Therefore, brain and placenta were the 2 sample types with significantly higher viral load than the rest and were ideal for molecular detection of JEV infection in piglets.

We also found a significant correlation between the viral antigen score of the frontal and parietal/temporal cortex and the molecular test results (the C_t value of the RT-qPCR test), by performing a Spearman correlation analysis ($r = -.5179$ and $-.4485$, respectively; P values = .0114 and .0363, respectively; Supplemental Fig. S4a, b). No such correlation was found in other regions of the CNS.

Discussion

This study reports a detailed, multidisciplinary laboratory investigation of the first major outbreak of JEV in pigs in mainland Australia. Orthoflavivirus infection affected up to 100% of piglets *in utero* such that most were stillborn. The main neuropathologic feature was hydranencephaly, while porencephaly was also observed. Occasionally these malformations were accompanied by arthrogryposis, scoliosis, and kyphosis, and myelodysplasia was present in several piglets. Only a minority of animals were born alive, sometimes showing signs of neurologic disease. Diagnostically, the brain and placenta were the 2 samples with the highest viral genomic load, and therefore, the best samples for molecular detection of fetal JEV infection.

The fetal CNS was the major target for JEV infection in pregnant sows and resulted in a mixed picture of failed

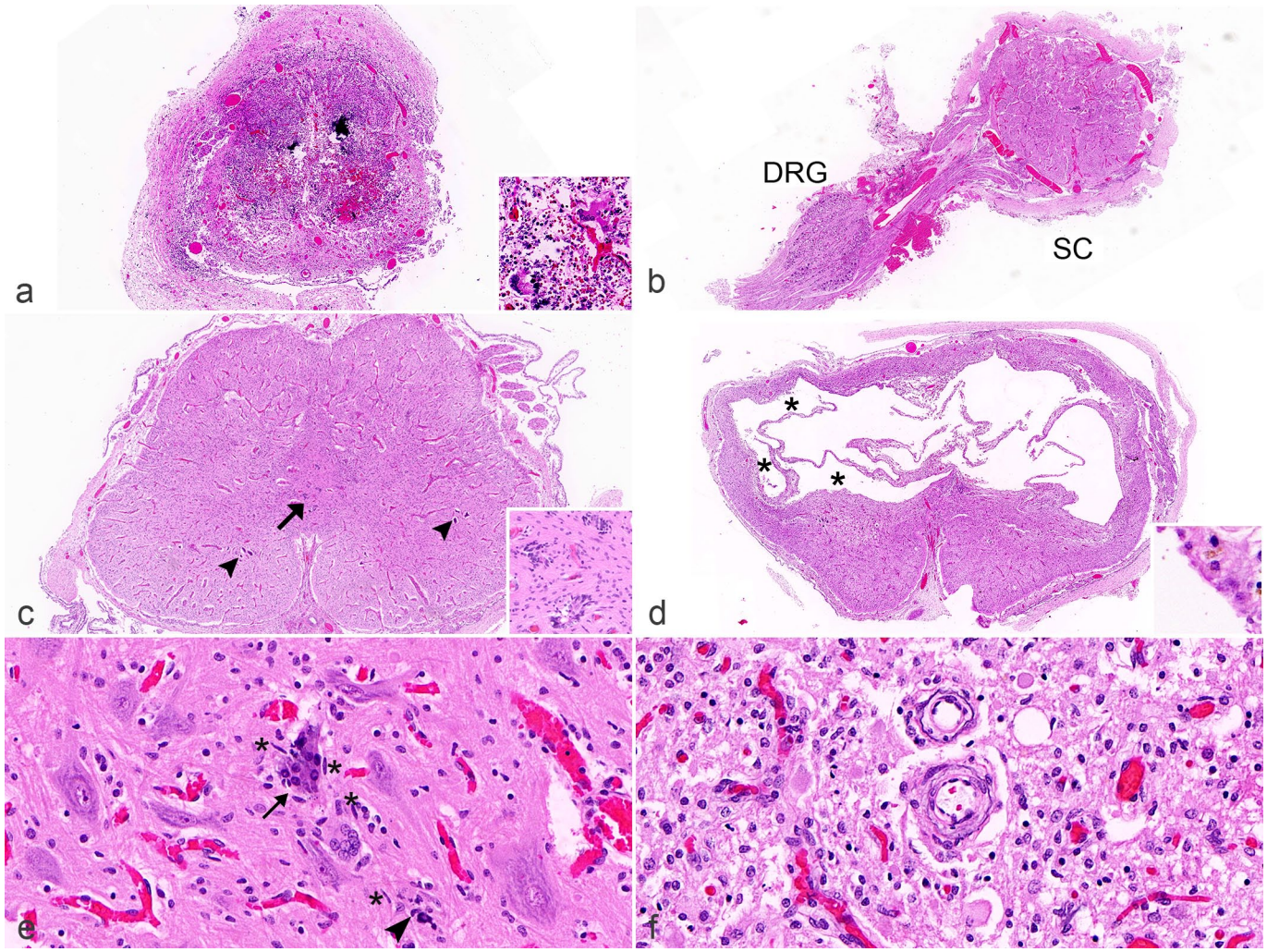

Figure 4. Histopathologic changes in the spinal cord of Japanese encephalitis virus (JEV)-positive porcine fetuses. Hematoxylin and eosin. (a) Cervical spinal cord. Normal gray and white matter distinction is inapparent due to severe diffuse myelomalacia with multifocal parenchymal calcification and hemorrhage. The spinal meninges are also thickened. Inset: multinucleated giant cells likely in response to the mineral deposits. (b) Cervical spinal cord. The relatively small size of the spinal cord (SC) as compared with the size of the adjacent dorsal root ganglion (DRG) is interpreted as micromyelia. (c) Cervical spinal cord. Myelodysplasia evident in this cord is characterized by the presence of multiple profiles of the central canal (duplication; arrow), a dysplastic gray matter, and bifurcation of the ventral median fissure. Bilaterally, only 2–3 basophilic mineralized motor neurons (arrowheads) are in the ventral horns. Inset: Higher magnification of the disorderly replicates of the central canal. (d) Cervical spinal cord. Replacing much of the dorsal half of this spinal cord is a cavity with several communicating compartments, some of which are partially lined by ependymal cells, while others lack an ependymal lining (*). This was interpreted as syringohydromyelia. Inset: A compartment within the cavity that is lined by ependymal cells with an eosinophilic brush border. (e) Ventral horn of the lumbar spinal cord. The motor neuron indicated by the arrow is undergoing active neuronophagia, while the arrowhead indicates a mineralized cell, presumably a residual neuron, at the center of another focus of neuronophagia. In between these 2 neurons is a multinucleated giant cell. Also note the presence of several rod-shaped nuclei of reactive microglial cells, sometimes close to neuronophagic foci (*). (f) Lumbar spinal cord. Two blood vessels have concentric mural deposits of basophilic mineral.

or disturbed neurodevelopment, admixed with degenerative, necrotizing, and inflammatory changes. Hydranencephaly observed in the JEV-infected porcine fetuses bears many similarities to that of other animals infected with neuroteratogenic viruses, such as those belonging in the genera *Pestivirus* (*Flaviviridae*), *Orthobunyavirus* (*Peribunyaviridae*), and *Rubulavirus* (*Paramyxoviridae*).[4,22,34,35,48] The pathogenesis in many of these infections is well studied. Briefly, virus-induced hydranencephaly has been shown to result from infection and destruction of the germinal plate which leads to necrosis of neuroprogenitor cells and early differentiated cells with subsequent hypoplasia, atrophy, and even dysplasia of developing structures, such as the cerebrum.[48] The JEV-infected porcine fetuses reported here showed evidence of viral tropism for neurons in the neocortex resulting in necrosis of neurons and atrophy/hypoplasia of the dorsal cerebrum, where the viral burden was heaviest. These findings suggest a similar pathogenesis as proposed for other neuroteratogenic viral infections. However,

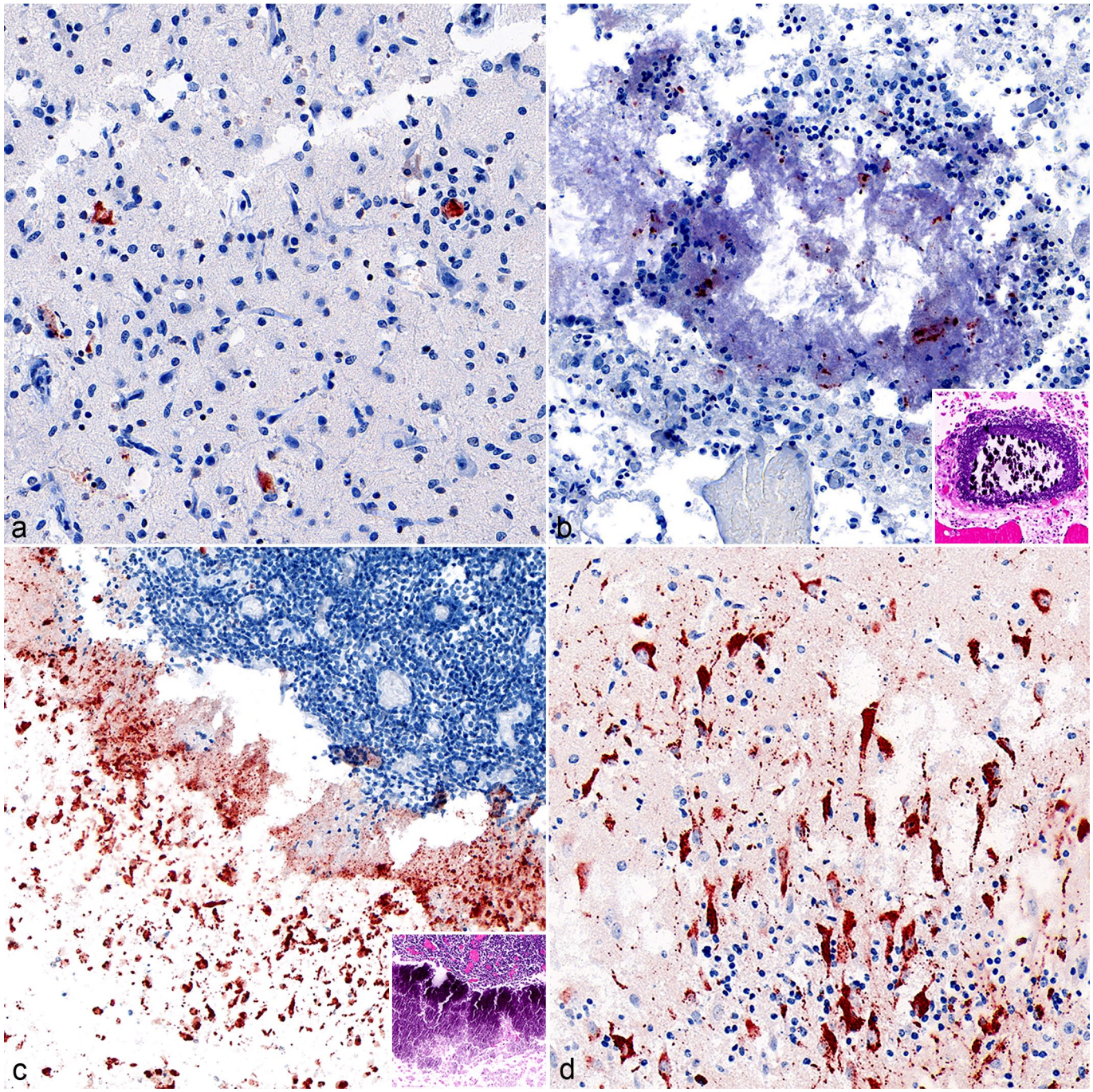

Figure 5. Japanese encephalitis virus detection by immunohistochemistry (IHC) using antibody targeting flaviviral NS1 antigen. (a) Midbrain. A few IHC-positive cells are evident in a background of diffuse, mild polioencephalitis. Clustering of mononuclear cells around the antigen-positive cell at right is consistent with neuronal infection and satellitosis. For comparison, note size and shape of the intact neuron below. (b) Dorsal cerebrum. A midfield ovoid focus of amorphous, mineralized parenchyma contains a few clusters of antigen-positive cell debris. Inset: The corresponding mineralized focus on the hematoxylin and eosin (HE)-stained section. (c) Cerebral cortex. Numerous, intact, antigen-positive cells and other necrotic cells clustered together, subjacent to a diffuse mononuclear meningeal infiltrate. Inset: Corresponding area of the necrotic and mineralized cortex in the HE-stained section. (d) Cerebral cortex. Numerous neurons with prominent cytoplasmic labeling including punctate swellings along neurites ("varicosities") within a background of diffuse, mild inflammation.

cases of hydranencephaly and other CNS malformations, not associated with an infectious agent, are well known and can show a familial pattern.[42] In such cases, a vascular-mediated pathogenesis has been proposed, either by impaired vasculogenesis predisposing areas of the developing CNS to injury, or through direct vascular injury (vasculopathy).[6] Furthermore, a viral-associated vascular basis for hydranencephaly has been proposed in some bovine fetuses, such as those experimentally inoculated

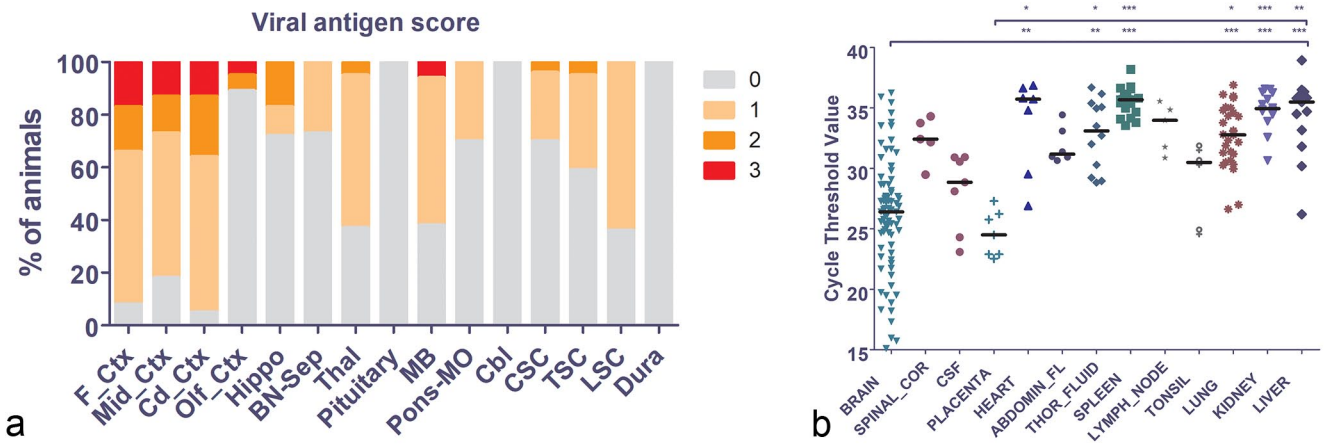

Figure 6. Japanese encephalitis virus (JEV) antigen distribution in the central nervous system and molecular detection in diagnostic samples. (a) Proportional stacked bar graph of the immunohistochemistry score for viral antigen across the different regions of the brain and spinal cord (*x*-axis), expressed as % of animals with the different scores on the *y*-axis. The different colors represent the different antigen scores and are indicated by the legend on the right of the graph. The proportion of infected cells was highest in the first 3 bars representing the neocortex. In contrast, infection in the phylogenetically older olfactory cortex was very low. Abbreviations: F_Ctx, frontal lobe; Mid_Ctx, parietal/temporal lobe; Cd_Ctx, caudal parietal/occipital lobe; Olf_Ctx, olfactory cortex; Hippo, hippocampus; BN-Sep, basal nuclei and septum; Thal, thalamus; MB, midbrain; Pons-MO, pons/medulla oblongata; Cbl, cerebellum; CSC, cervical spinal cord; TSC, thoracic spinal cord; LSC, lumbar spinal cord; dura, dura mater. (b) Scatterplot of the cycle threshold (C_t) values from the JEV quantitative reverse transcriptase PCR performed on a variety of sample types. Brain and placenta were the 2 sample types with the lowest median C_t values (ie, highest viral load), suggesting their suitability for molecular detection of JEV infection in affected piglets. Each dot represents the C_t value of one sample. The horizontal bar represents the median C_t value per sample type. Abbreviations: SPINAL_COR, spinal cord; CSF, cerebrospinal fluid; ABDOMIN_FL, abdominal fluid; THOR_FLUID, thoracic fluid. Statistical significance of the comparisons was denoted by: $^*P < .05$; $^{**}P$ value $< .01$; $^{***}P < .001$.

with bluetongue virus in utero.[27] In that context, the microvascular mineralization described here in the brain of JEV-infected piglets may contribute to the neural injury.

Injury to the brain, both in utero and in the postnatal period, often results in necrosis and mineralization. Tissue destruction with mineralization was a common finding in this study. In contrast, the vascular mineralization found in a minority of JEV-infected piglets is an unusual finding, which has not been previously reported in cases of porcine JEV.

Variation in the severity of hydranencephaly was a feature noted in the JEV-infected piglets examined in this study. Similarly, variation in the crown-to-rump length, degree of carcass preservation (eg, presence of mummification), and CNS viral burden were also noted. There are several potential explanations for such variations and included, but are not limited to, the following. (1) In utero infection at different gestational stages. Early brain infection would expose progenitor and newly formed, immature neurons at a time when host inflammatory and immune responses are limited or lacking. JEV primarily infects immature (rather than mature, differentiated) neurons,[1,8,33] and a window of highest susceptibility at 40–54 days of gestation (mid-gestation) has been proposed for causing reproductive failure, fetal viremia, and CNS pathologic changes.[7,45] Infection of differentiated neural cells later in gestation would be less disruptive of normal development. (2) Different doses of the virus delivered transplacentally to the fetal circulation and subsequently to the CNS, where presumably higher doses would lead to more widespread CNS infection and in turn necrosis of the neuroparenchyma. (3) Variation in maternal disease, such as degree and length of maternal pyrexia, which may influence normal CNS development (potentially teratogenic). (4) The potential role of different viral variants that may have circulated during the outbreak. Different viral variants could account for subtle differences in the clinical and pathologic manifestations of the disease across the country. Controlled challenge experiments in pregnant sows would be required to understand why some areas of the brain appeared to be targeted and others spared and the interplay of fetal age, viral variants, and the protective or contributory roles of the inflammatory responses.

Micromyelia and myelodysplasia were 2 major pathologic changes observed in the spinal cord of the JEV-infected fetuses. Micromyelia without myelodysplasia has been reported in Schmallenburg virus-infected newborn calves, and was largely attributed to the failure of normal development of the spinal ventral horn.[4] We found an association between fetal JEV infection, myelodysplasia, and arthrogryposis, presumably due to the loss of and/or malformed ventral horn; a link that has also been established in Schmallenburg virus and Akabane virus-infected ruminants.[36,48] Of interest, myelodysplasia has often been reported to have a non-infectious basis, such as genetic abnormalities or ingestion of neuroteratogenic plants.[34,48] While the literature has noted a common association between spinal cord malformations and vertebral abnormalities (eg, scoliosis and kyphosis), this link was less consistent in the JEV-infected fetuses in this study, or at least not as consistent

as that between myelodysplasia and arthrogryposis.[48] Further examination into the pathogenesis of the vertebral abnormalities is warranted.

This study revealed that fresh samples of the fetal brain and placenta contained the highest JEV genomic load, and thus, are ideal samples for molecular detection of JEV infection in a diagnostic setting. Our IHC results suggest that sampling of the dorsal neopallium (ie, cerebral cortex) should optimize virus detection by RT-qPCR and IHC, as compared with other CNS sites (Fig. 6a and Supplemental Fig. S4). If the cerebrum is reduced to a thin membrane with minimal parenchyma available, other CNS sites, such as the thalamus, midbrain, or lumbar spinal cord should also provide positive molecular detection, but likely with lower viral burden (Fig. 6a).

Some fresh placentas were collected for molecular detection in this outbreak; however, the samples were often in suboptimal condition for pathologic assessment. While beyond the scope of the current study, we acknowledge that a thorough pathologic examination of the porcine placenta in JEV-positive fetuses would provide a more comprehensive characterization of the disease. Transplacental transfer of the virus is the route to fetal infection. Past studies have shown that flaviviruses, such as Zika virus, can infect Hofbauer cells (placental macrophages), placental fibroblasts, endothelial cells, amniotic epithelial cells, and trophoblasts.[21,28,32,38,49] Zika viral infection in the placenta was associated with chronic inflammation and was implicated in the destruction of villous architecture and trophoblastic epithelium, and thus facilitated passage of the virus to the fetal circulation.[32,41] We currently do not have an insight into for the mechanism of JEV infection at the maternal-fetal interface.

The hemorrhagic and edematous lesions noted in extraneural tissues were flaviviral antigen negative on IHC, despite positive RT-qPCR results in some tissues. While we acknowledge the inherently lower sensitivity of IHC than RT-qPCR in detecting viral infections, we interpreted these extraneural lesions as nonspecific with respect to JEV infection, since similar lesions have been noted in porcine stillbirths of other causes.[46] The positive signal detected by RT-qPCR could simply reflect fragments of viral RNA in circulation, for example, due to a residual fetal viremia.

The explosive nature of the JEV outbreak and the high rate of reproductive failure in pigs described here was unprecedented in Australia; it was the first report of ongoing JEV infections on the Australian mainland, which appeared almost simultaneously over the range. At that time, the national domestic pig herds were naïve to JEV and highly susceptible to infection. The effect of this outbreak on future incidence of JEV infection in Australia is difficult to predict. While sows that lost their litters were largely clinically unaffected and would expect to have some degree of immunity to reinfection, their relatively short productive lifespan in commercial piggeries and thus the regular introduction of JEV-naïve gilts into the productive herd may pose an increased risk of another widespread outbreak. Abundance of JEV in mosquitoes and potential reservoir hosts, recent evidence suggesting horizontal transmission between pigs,[39] and the warming climate are also factors to consider in determining the likelihood of another severe outbreak.

Despite this uncertainty, it was clear that the early recognition of the clinicopathologic profile and the prompt testing of multiple piglet tissues from JEV-infected pig herds facilitated an effective national response to the 2022 Australian JEV outbreak. Our study provided the pathologic perspective of the outbreak, demonstrating that hydranencephaly and porencephaly were the most common CNS abnormalities observed in JEV-positive piglets, enabling veterinary and allied one health professionals to recognize this condition promptly and initiate the appropriate response for future outbreaks. As of February 2023, there were 46 reported human cases of JEV with 7 deaths, and surveillance efforts in piggeries, mosquitos, and sentinel chickens detected continued JEV activity in the Murray River region of eastern Australia.[29] It is anticipated that JEV will likely continue to pose a significant threat to the Australian pig industry as well as human health.

Acknowledgements

We would like to acknowledge Dr Heather Smith (PIRSA biosecurity), and Dr Ian Jerrett and Dr. Mark Hawes (AgVic AgriBio); Dr Anita Gordon, Dr Kathryn Markham, Dr Wafa Shinwari, and the BSL molecular diagnostics staff (BSL); The EMAI, NSW, DPIRD histology team, and specimen receival and virology team; Northern Australia Quarantine Strategy (NAQS); Dr Helle Bielefeldt-Ohmann; and the ACDP histology, molecular, sequencing, virology, and duty vet teams for their contributions to the investigation and/or discussion of the JEV outbreak cases. We also acknowledge the field veterinarians for discussions and submission of case materials.

Authors' Contributions

WWS, AJ, DF, PK, JP, DTW, JB, and PP designed the experiments and study; WWS, AJ, LKM, SO, SAT, EL, ZS, ALN, MH, DF, PK, CS, JP, JH, KM, YG, TE, JB, and PP performed necropsies and/or experiments; WWS, AJ, LKM, ALN, CS, RP, BAS, and PP performed histologic evaluations; WWS, AJ, LKM, SO, SAT, GK, TR, JB, BAS, and PP collected and analyzed data; WWS, AJ, SO, EL, JH, KM, DTW, RP, JB, BAS, and PP wrote the manuscript; and all authors reviewed the manuscript.

Declaration of Conflicting Interests

The author(s) declared no potential conflicts of interest with respect to the research, authorship, and/or publication of this article.

Funding

The author(s) received no financial support for the research, authorship, and/or publication of this article.

ORCID iDs

Willy W. Suen https://orcid.org/0000-0002-4544-6773
Leah K. Manning https://orcid.org/0000-0002-1609-4772
Angel L. Ngo https://orcid.org/0009-0005-0148-4603

Mark Hazelton https://orcid.org/0000-0002-2224-401X
Deborah Finlaison https://orcid.org/0000-0003-2639-4880
Peter Kirkland https://orcid.org/0000-0001-8026-4185
Cathy Shilton https://orcid.org/0000-0001-6513-6273
Tristan Reid https://orcid.org/0000-0001-6150-3566
David T. Williams https://orcid.org/0000-0002-7169-149X
Richard Ploeg https://orcid.org/0000-0001-6482-8366
Brian A. Summers https://orcid.org/0000-0002-5092-707X
Pedro Pinczowski https://orcid.org/0000-0002-9210-6026

References

1. Ariff IM, Thounaojam MC, Das S, et al. Japanese encephalitis virus infection alters both neuronal and astrocytic differentiation of neural stem/progenitor cells. *Journal of Neuroimmune Pharmacology: the Official Journal of the Society on Neuroimmune Pharmacology*. 2013;**8**:664–676.
2. Au GG, Marsh GA, McAuley AJ, et al. Characterisation and natural progression of SARS-CoV-2 infection in ferrets. *Scientific Reports*. 2022;**12**:5680.
3. Bancroft JD, Gamble M. *Theory and practice of histological techniques*. 5th ed. London: Churchill Livingston; 2002.
4. Bayrou C, Garigliany MM, Sarlet M, et al. Natural intrauterine infection with Schmallenberg virus in malformed newborn calves. *Emerging Infectious Diseases*. 2014;**20**:1327–1330.
5. Campbell GL, Hills SL, Fischer M, et al. Estimated global incidence of Japanese encephalitis: a systematic review. *Bulletin of the World Health Organization*. 2011;**89**:766–774; 774a–774e.
6. Cantile C, Youssef S. Chapter 4—Nervous system. In: Maxie MG, ed. *Jubb, Kennedy & Palmer's Pathology of Domestic Animals: Volume 2*. 6th ed. Philadelphia, PA: W.B. Saunders; 2016:273
7. Chapagain S, Pal Singh P, Le K, et al. Japanese encephalitis virus persists in the human reproductive epithelium and porcine reproductive tissues. *Plos Neglected Tropical Diseases*. 2022;**16**:e0010656.
8. Das S, Basu A. Japanese encephalitis virus infects neural progenitor cells and decreases their proliferation. *Journal of Neurochemistry*. 2008;**106**:1624–1636.
9. Davies ES, Volk HA, Behr S, et al. Porencephaly and hydranencephaly in six dogs. *The Veterinary Record*. 2012;**170**:179.
10. Desai A, Shankar SK, Ravi V, et al. Japanese encephalitis virus antigen in the human brain and its topographic distribution. *Acta Neuropathologica*. 1995;**89**:368–373.
11. Desingu PA, Ray PK, Patel BH, et al. Pathogenic and genotypic characterization of a Japanese encephalitis virus isolate associated with reproductive failure in an Indian pig herd. *PLoS ONE*. 2016;**11**:e0147611.
12. Ellis PM, Daniels PW, Banks DJ. Japanese encephalitis. *The Veterinary Clinics of North America Equine Practice*. 2000;**16**:565x–578xi.
13. Fu TL, Ong KC, Wong KT. Pathological findings in a mouse model of Japanese encephalitis infected via the footpad. *Neurology Asia*. 2015;**20**:349–354.
14. German AC, Myint KS, Mai NT, et al. A preliminary neuropathological study of Japanese encephalitis in humans and a mouse model. *Transactions of the Royal Society of Tropical Medicine and Hygiene*. 2006;**100**:1135–1145.
15. Hanna JN, Ritchie SA, Phillips DA, et al. An outbreak of Japanese encephalitis in the Torres Strait, Australia, 1995. *The Medical Journal of Australia*. 1996;**165**:256–260.
16. Hanna JN, Ritchie SA, Phillips DA, et al. Japanese encephalitis in north Queensland, Australia, 1998. *The Medical Journal of Australia*. 1999;**170**:533–536.
17. Harrington DG, Hilmas DE, Elwell MR, et al. Intranasal infection of monkeys with Japanese encephalitis virus: clinical response and treatment with a nuclease-resistant derivative of poly (I).poly (C). *The American Journal of Tropical Medicine and Hygiene*. 1977;**26**:1191–1198.
18. Hase T, Dubois DR, Summers PL. Comparative study of mouse brains infected with Japanese encephalitis virus by intracerebral or intraperitoneal inoculation. *International Journal of Experimental Pathology*. 1990;**71**:857–869.
19. Iglesias R: Outbreak of Japanese encephalitis in Australia. In: Animal Health Surveillance Quarterly Report, pp. 4–6. Animal Health Australia; 2022.
20. Johnson RT, Burke DS, Elwell M, et al. Japanese encephalitis: immunocytochemical studies of viral antigen and inflammatory cells in fatal cases. *Annals of Neurology*. 1985;**18**:567–573.
21. Jurado KA, Simoni MK, Tang Z, et al. Zika virus productively infects primary human placenta-specific macrophages. *JCI Insight*. 2016;**1**:e88461.
22. Kessell A, Finnie J, Windsor P. Neurological diseases of ruminant livestock in Australia. IV: viral infections. *Australian Veterinary Journal*. 2011;**89**:331–337.
23. Kumar R, Tripathi P, Singh S, et al. Clinical features in children hospitalized during the 2005 epidemic of Japanese encephalitis in Uttar Pradesh, India. *Clinical Infectious Diseases: an Official Publication of the Infectious Diseases Society of America*. 2006;**43**:123–131.
24. Kuwata R, Torii S, Shimoda H, et al. Distribution of Japanese encephalitis virus, Japan and southeast Asia, 2016-2018. *Emerging Infectious Diseases*. 2020;**26**:125–128.
25. Mackenzie JS, Williams DT. Japanese encephalitis virus: an emerging and re-emerging virus in Australia. *Microbiology Australia*. 2022;**43**:150–155.
26. Mackenzie JS, Williams DT, van den Hurk AF, et al. Japanese encephalitis virus: the emergence of genotype IV in Australia and its potential endemicity. *Viruses*. 2022;**14**:2480.
27. MacLachlan NJ, Osburn BI. Bluetongue virus-induced hydranencephaly in cattle. *Veterinary Pathology*. 1983;**20**:563–573.
28. Martines RB, Bhatnagar J, de Oliveira Ramos AM, et al. Pathology of congenital Zika syndrome in Brazil: a case series. *Lancet (London, England)*. 2016;**388**:898–904.
29. McGuinness SL, Lau CL, Leder K. The evolving Japanese encephalitis situation in Australia and implications for travel medicine. *Journal of Travel Medicine*. 2023;**30**:taad029.
30. Miyake M. The pathology of Japanese encephalitis. A review. *Bulletin of the World Health Organization*. 1964;**30**:153–160.
31. Myint KS, Raengsakulrach B, Young GD, et al. Production of lethal infection that resembles fatal human disease by intranasal inoculation of macaques with Japanese encephalitis virus. *The American Journal of Tropical Medicine and Hygiene*. 1999;**60**:338–342.
32. Noronha L, Zanluca C, Azevedo ML, et al. Zika virus damages the human placental barrier and presents marked fetal neurotropism. *Memorias Do Instituto Oswaldo Cruz*. 2016;**111**:287–293.
33. Ogata A, Nagashima K, Hall WW, et al. Japanese encephalitis virus neurotropism is dependent on the degree of neuronal maturity. *Journal of Virology*. 1991;**65**:880–886.
34. Peperkamp NH, Luttikholt SJ, Dijkman R, et al. Ovine and bovine congenital abnormalities associated with intrauterine infection with Schmallenberg virus. *Veterinary Pathology*. 2015;**52**:1057–1066.
35. Philbey AW, Ross AD, Kirkland PD, et al. Skeletal and neurological malformations in pigs congenitally infected with Menangle virus. *Australian Veterinary Journal*. 2007;**85**:134–140.
36. Polledo L, García Marín JF, Martínez-Fernández B, et al. Recurrent outbreaks of myelodysplasia in newborn calves. *Journal of Comparative Pathology*. 2012;**147**:479–485.
37. Pyke AT, Williams DT, Nisbet DJ, et al. The appearance of a second genotype of Japanese encephalitis virus in the Australasian region. *The American Journal of Tropical Medicine and Hygiene*. 2001;**65**:747–753.
38. Quicke KM, Bowen JR, Johnson EL, et al. Zika virus infects human placental macrophages. *Cell Host & Microbe*. 2016;**20**:83–90.
39. Ricklin ME, García-Nicolás O, Brechbühl D, et al. Vector-free transmission and persistence of Japanese encephalitis virus in pigs. *Nature Communications*. 2016;**7**:10832.

40. Ritchie SA, Rochester W. Wind-blown mosquitoes and introduction of Japanese encephalitis into Australia. *Emerging Infectious Diseases*. 2001;**7**:900–903.
41. Roberts DJ, Frosch MP. Zika and histopathology in first trimester infections. *Lancet (London, England)*. 2016;**388**:847–849.
42. Schild AL, Fiss L, Damé MC, et al. Congenital hydranencephaly and cerebellar hypoplasia in water buffalo in southern Brazil. *Journal of Veterinary Diagnostic Investigation: Official Publication of the American Association of Veterinary Laboratory Diagnosticians*. 2011;**23**:603–609.
43. Sethi M, Das T, Tomar N, et al. Japanese encephalitis virus-induced neuropathology in mouse model infected through the conjunctival route. *The Indian Journal of Medical Research*. 2019;**150**:498–503.
44. Shao N, Li F, Nie K, et al. Taqman real-time RT-PCR assay for detecting and differentiating Japanese encephalitis virus. *Biomedical and Environmental Sciences*. 2018;**31**:208–214.
45. Shimizu T, Kawakami Y, Fukuhara S, et al. Experimental stillbirth in pregnant swine infected with Japanese encephalitis virus. *The Japanese Journal of Experimental Medicine*. 1954;**24**:363–375.
46. Sims LD, Glastonbury JRW. Neonatal mortality. In: Sims LD and Glastonbury JRW (eds) *The pathology of the pig: a diagnostic guide*. Barton, ACT, Australia: The Pig Research and Development Corporation; 1996:425.
47. Solomon T, Dung NM, Kneen R, et al. Japanese encephalitis. *Journal of Neurology, Neurosurgery, and Psychiatry*. 2000;**68**:405–415.
48. Summers BA, Cummings JF, DeLahunta A. *Veterinary Neuropathology*. St. Louis, MI: Mosby; 1995.
49. Tabata T, Petitt M, Puerta-Guardo H, et al. Zika virus targets different primary human placental cells, suggesting two routes for vertical transmission. *Cell Host & Microbe*. 2016;**20**:155–166.
50. Takashima I, Watanabe T, Ouchi N, et al. Ecological studies of Japanese encephalitis virus in Hokkaido: interepidemic outbreaks of swine abortion and evidence for the virus to overwinter locally. *The American Journal of Tropical Medicine and Hygiene*. 1988;**38**:420–427.
51. Tsubaki S, Masu S, Obata Y, et al. Studies on Japanese B. encephalitis on swine encephalitis and abortion (1947-1949). *The Kitasato Archives of Experimental Medicine*. 1950;**23**:9–12.
52. Van Den Hurk AF, Johansen CA, Zborowski P, et al. Mosquito host-feeding patterns and implications for Japanese encephalitis virus transmission in northern Australia and Papua New Guinea. *Medical and Veterinary Entomology*. 2003;**17**:403–411.
53. van den Hurk AF, Pyke AT, Mackenzie JS, et al. Japanese encephalitis virus in Australia: from known known to known unknown. *Tropical Medicine and Infectious Disease*. 2019;**4**:38.
54. Watanabe M. Incidence, diagnosis and control of Japanese encephalitis in pigs in Japan, with reference to stillbirth. Appendix: HVJ in pig especially with stillbirth in Japan. *Japan Agricultural Research Quarterly*. 1968;**3**: 24–30.
55. Yamada M, Nakamura K, Yoshii M, et al. Brain lesions induced by experimental intranasal infection of Japanese encephalitis virus in piglets. *Journal of Comparative Pathology*. 2009;**141**:156–162.